Improving natural sunlight photocatalytic efficiency of ZnO nanowires decorated by iron oxide cocatalyst via a simple drop method

Marie Le Pivert, Hongri Suo, Gang Tang, Han Qiao, Zhicheng Zhao, Nathan Martin, Chongxuan Liu, Yamin Leprince-Wang

Improving natural sunlight photocatalytic efficiency of ZnO nanowires decorated by iron oxide cocatalyst via a simple drop method

Marie Le Pivert [a], Hongri Suo [b,c], Gang Tang [b,c], Han Qiao [b,c], Zhicheng Zhao [d], Nathan Martin [a], Chongxuan Liu [b,c], Yamin Leprince-Wang [a]*,

[a] ESYCOM, Univ Gustave Eiffel, CNRS (UMR 9007), F-77454 Marne-la-Vallée, France

[b] State Environmental Protection Key Laboratory of Integrated Surface Water-Groundwater Pollution Control, School of the Environmental Science and Engineering, Southern University of Science and Technology, Shenzhen, 518055, China

[c] Guangdong Provincial Key Laboratory of Soil and Groundwater Pollution Control, School of Environmental Science and Engineering, Southern University of Science and Technology, Shenzhen, 518055, China

[d] Foshan (Southern China) Institute for New Materials, Foshan, 528200, China

* Corresponding author: Yamin Leprince-Wang (yamin.leprince@univ-eiffel.fr), Tel. +33 1 60 95 72 76 Cité Descartes 5 Bd. Descartes, Champs-sur-Marne 77454 Marne-la-Vallée Cedex 2, France.

Abstract:

In this study, iron oxide cocatalysts were deposited on the surface of ZnO nanostructures by a simple "drop, evaporation, calcination" method. Different deposition concentrations were studied, allowing to extend the photocatalyst absorption spectral range from UV to visible light, improving the photocatalytic efficiency under natural sunlight. An optimal deposition concentration of 0.06% molar percentage of iron against zinc led to improve by 11% the Methyl Orange (MO) photocatalytic degradation after 5h under natural sunlight. No iron leaching was detected by ICP-MS analysis after the water purification by photocatalysis. By studying the lifetime stability of the optimal sample under a powerful UV light source, no losses of photocatalytic efficiency were recorded after several degradation cycles. Nevertheless, under this powerful light source, photocorrosion damages were observed with two antagonistic effects: (1) no photocorrosion effect for the ZnO regions covered by iron oxide and (2) ZnO photocorrosion and an acceleration of the dissolution of the ZnO nanostructures in uncovered regions. Thus, we assume the electron/hole delocalisation, which is responsible of the photocatalytic activity improvement, is also the reason justifying the ZnO photocorrosion acceleration of uncovered part. The photocorrosion phenomena was observed only under the powerful UV light source, not under natural sunlight.

Keywords: Zinc Oxide, Iron oxide, Nanostructures, Cocatalyst, Photocatalysis, Water depollution.

1. Introduction

It is increasingly recognized that pollution is a major issue especially in every urban center. Hence, to solve this problem, developing and designing smart materials for environmental depollution becomes a promising solution. For those reasons, photocatalytic infrastructures appear as a promising air and water purification method due to their abilities to degrade and mineralize toxic organic pollutants into harmless compounds as H_2O, CO_2, NO_3^- [1-5].

For developing these new materials, the traditional synthesis need to be adapted and optimized, in order to accommodate certain conditions. First, the synthesis may not damage building construction materials. It implies soft synthesis conditions, which often have the advantage of being more easily scaled-up and respectful towards the environment. Indeed, the production process as well as the used photocatalyst should be as environmentally friendly as possible. Therefore, the photocatalyst has to be efficiently fixed on the construction material surface in order to avoid any release in the environment. For all those reasons, we propose to implement ZnO nanostructures onto civil engineering material surfaces by a low cost direct hydrothermal growth, in order to obtain photocatalytic concretes and tilings, whose good photocatalytic efficiencies were already proved in our previous works [6,7]. In fact, ZnO is a promising photocatalyst due to its good thermal and chemical stabilities, its non-toxicity [8], its low-cost as a raw material, its wide bandgap (> 3.3 eV) and its band-level potential energy, allowing water photooxydation and dioxygen photoreduction for pollutant photocatalytic degradation.

Nevertheless, its wide bandgap is also a limitation for visible-light absorption. Thus, numerous strategies to extend ZnO light absorption have been developed, as doping ZnO by adding Fe, Co, or Ag during the synthesis [9]. Unfortunately, this method, for which the efficiency was already demonstrated [9-11], could not be applied on construction materials due to some possible interaction between the non-conventional substrate and the dopant ions and an adverse effect on the photocatalytic efficiency under natural sunlight for Acid Red 14 degradation (Figure 1). In fact, in

recent works, we demonstrated that construction materials, for instance concrete, could influence ZnO growth and morphology due to some local pH and chemical composition modification on its chaotic surface [7]. Thus, for this application, it is imperative to develop a post-grown ZnO doping method in order to reduce contact between the substrate and the doping solution.

Before studying this approach at large scale on construction substrate, the relevance of this solution was evaluated at the laboratory scale on silicon (Si) surfaces to have better control and understanding. In the present work, Fe(III) ion was selected to improve the ZnO nanowires (NWs) light-absorption and photocatalytic activity, owing to its low-cost and relative eco-friendly properties. Fe(III) solution was dropped on ZnO nanowires grown onto Si, then dried and calcined. The iron concentration influence on ZnO NWs microstructure and their optical properties was studied using scanning electron microscope (SEM), UV–visible spectrophotometry (UV-vis), X-ray diffraction (XRD), and inductively coupled plasma mass spectrometry (ICP-MS). The optimum sample was then selected for Methyl Orange (MO) photocatalytic degradation under natural sunlight to investigate the Fe(III) doped ZnO NWs' photocatalytic efficiency. Optimum sample lifetime and photocorrosion were also studied in this work.

2. Materials and methods

2.1 ZnO nanowires synthesis

ZnO NWs were synthesized on Si substrate ((100) ± 0.5°) by a simple two-step hydrothermal method. After a substrate cleaning process [12], a seed layer solution, obtained by mixing 10 g of poly-vinyl alcohol (PVA) (99%, Aldrich) and 1 g of zinc acetate dihydrate in 100 mL deionized water (DI water), was spin-coated onto one side of a Si surface (1,3 cm × 1,5 cm) (3000 rpm, 1 min). The thin film was then calcined at 500°C for 3 hours in ambient atmosphere in order to remove the PVA and form ZnO nanocristallites as seeds, which will act as nucleation centers to promote the homogeneous growth of ZnO NWs in the second step. ZnO NWs were grown at 90°C during 4 hours into a Teflon sealed reactor containing an equimolar aqueous solution

of zinc acetate dihydrate ($Zn(Ac)_2 \cdot 2\ H_2O$) (zinc acetate dihydrate, 99%, VWR) and hexamethylenetetramine (HMTA, ≥ 99%, VWR) at 0.025 M. At the end of the growing process, the Si substrates covered by ZnO nanowires (1.55 cm^2) were washed with DI water, dried under hot airflow (~30s at ~53°C), and post-annealed in an oven at 350°C for 30 minutes in ambient atmosphere in order to improve the ZnO crystallinity.

2.2 ZnO nanowires decoration with iron oxide

The iron oxide layer was deposited on ZnO nanowires post-growth by a simple drop method. A volume of 69.8 µL of $Fe(NO_3)_3$ (98%, Sigma-Aldrich), whose iron concentration range is included between $8{,}9 \times 10^{-9}$ mol and $4{,}5 \times 10^{-7}$ mol, was applied on the sample surface before a drying at 50°C for 30 min in an oven. Finally, the sample was annealed at 350°C for 1 hour in ambient atmosphere in order to convert and fix the iron oxide on ZnO surface.

The optical absorption spectrum was measured using a UV-Vis-NIR spectrophotometer (Lambda 750) equipped with an integrating sphere. Samples were also thoroughly characterized by SEM equipped with an energy dispersive spectroscopy (EDS) analyzer (Zeiss FE-SEM NEON 40; Zeiss Merlin), XRD (CuKα, λ = 1.5418 Å, Rigaku Smartlab), and ICP-MS (ICP-MS 7700, Agilent technologies). Samples will be labelled as the following: ZnO for the reference without iron deposition and ZnO-Fe% for modified samples. The iron deposited molar percentages were estimated using ICP-MS after the photocatalysis experiments and compared to the theoretical deposition. In order to perform the ICP-MS measurements, the samples were broken in two identical parts for conserving one part in order to repeat the measurement if necessary taking into account that ICP-MS is a destructive method. The total concentration was therefore estimated.

2.3 Photocatalysis experiments

Photodegradation of MO (85%, Sigma-Aldrich) was carried out between 10 AM and 15 PM under natural sunlight in an open atmosphere from November to December (in Shenzhen, China),

with the aim to find the optimal sample with the best photocatalytic efficiency. Modified samples were immerged in 15 mL of aqueous solution of MO with an initial concentration of 10 µM. Each experimentation day, a reference was recorded with the same ZnO sample, which was considered as a new sample thanks to a thermal reactivation (350°C, 30 min) before new test. The photocatalytic process with sunlight was monitored using UV-vis spectrophotometry (Agilent Cary-60) (Maya2000 Pro from Ocean Optics; Cary 60, Agilent) every 30 min for 5 h. Then, the degradation efficiency X(%) was estimated using Equation 1 :

$$X(\%) = \frac{A_0 - A}{A_0} \times 100\% \quad (1)$$

where A_0 and A stand for the initial and actual absorption peak values, respectively, at 464 nm.

To study the sample lifetime in reproducible conditions, 5 depollution cycles without thermal reactivation were carried out at the laboratory under a powerful UV light source (4500 mW/cm^2, λ = 365 nm, Hamamatsu LC8). Samples were immerged in 30 mL of an agitated aqueous solution of MO with an initial concentration of 10 µM and placed at 10 cm below the UV light source (35 mW/cm² on sample surface). The photocatalytic process was followed each 15 minutes considering that a faster degradation may be obtained due to the strong UV light intensity. Then, Equation 1 was used to calculate X(%).

3. Results and discussion

3.1 Characterisation

As shown on Figure 2a, highly homogeneous ZnO NWs, with length of 2.7 µm ± 0.4 µm, diameter of 65 nm ± 8 nm, and with a density of 2 × 10^9 NWs/cm², were synthetized, and no damage appeared on ZnO NWs modified by the iron ion droplet method. It is easily seen that the ZnO NWs seem to be covered by an iron oxide layer. This last observation is particularly true for the sample with high iron content and/or at the top of ZnO NWs, where long NWs gathered as a "tipis" shape. We strongly believe that "tipis" shape is the main reason explaining the non-

homogeneous iron oxide layer formation. However, the formed layer seems anchored with an intimate contact on ZnO NWs surface, which is very promising for a photocatalytic application without iron ions leaching.

Thereafter, optical properties were measured at room temperature using UV–vis spectrophotometry. Then, UV-vis spectrums were plotted with Tauc-Lorentz model (Figure 2b). As it can be observed, all the samples reveal an intense absorption under 400 nm corresponding to the bandgap of ZnO. Nevertheless, it is worth noting that the bandgap intensity decreases with the increase in iron content. Extrapolating from ZnO growth UV-vis real-time monitoring method [13], we assume that this bandgap intensity evolution is the marker for the iron oxide recovery on ZnO NWs. Associated with the decreasing bandgap intensity, we can note the gap value decreases from 3.27 eV for ZnO to 3.14 eV for the most iron modified sample (Table 1). Iron ion diffusion into the ZnO lattice thanks to zinc vacancy or interstitial sites could explain this trend. Nevertheless, iron ion (III) diffusion into ZnO lattice is known as weak. It is therefore possible to attribute the gap value evolution to the iron oxide layer presence. Moreover, this observation is consistent with the literature, where the same tendency in the presence of iron oxide has already been observed and attributed to the creation of an iron *s* atomic orbital (Fe_s) energy level below the conduction band (CB) of ZnO [14,15].

These explanations seem to be consistent with SEM observations and are fully in tune with the increase in visible light absorption related to the iron content. Visible light absorption is in line with the sample's colour evolution from blue/white to brick red/orange. The visible light evolution could also be explained by the d-d transition of Fe(III) in the FeOOH or in Fe_2O_3 [14-19]. The hypothesis of one of these oxides formation seems consistent with the brick red/orange sample coloration. Besides, Li *et al.* demonstrated that ZnO/TiO_2 surface was active for FeOOH nucleation and nano-sheet synthesis by a simple chemical bath deposition method in a $FeCl_2 \cdot 4\ H_2O$ (5 mM) aqueous solution at 40°C for 10 minutes [20]. By drawing a parallel with Shi *et al.* study [21], where

the calcination at different temperatures of FeOOH is investigated, we may suspect that FeOOH and Fe_2O_3 could coexist on the ZnO surface. Moreover, Achouri et *al.* assumed that ZnO acts as a support able to absorb $FeCl_3$ at its surface until its conversion into iron oxide (Fe_2O_3) through heating and annealing at 100°C [22].

Then, the ZnO hexagonal Wurtzite NWs were clearly identified on all XRD patterns without peaks shifting (Figure 2c). This result suggests that Fe(III) compounds were only fixed on the ZnO NWs surface and did not affect the ZnO lattice [19]. This finding is consistent with the idea of oxide formation on ZnO NWs. No related diffraction peaks of iron oxide were detected even for the high iron concentration samples. Indeed, we did not attribute the 2-theta 44 degrees reflection, which is not typical for ZnO Wurzite crystal structure, to iron oxide, due to its presence on unmodified ZnO. In some literature studies, this peak can also be identified on ZnO XRD pattern prepared with zinc acetate dehydrate salt [23,24]. This peak could be due to the acetate ion presence in the first nucleation layer deposition, which may be in excess in this layer. The low iron percentage, FeOOH dihydroxylation to from Fe_2O_3 and its poor crystallinity could explain this observation [22,25]. Besides, the lack of iron oxide XRD peaks was already noted in literature, while its presence can be proved by Raman or FT-IR characterization [15,17,22,26].

To investigate leaching and iron content on ZnO NWs, ICP-MS measurements were done after the photocatalysis experiments and compared to theoretical deposited concentration. From Table 1, it can be noted that a slight error between ICP-MS estimation and theoretical deposition concentration has been recorded. We assume that this low difference is not due to iron leaching during photocatalysis but could be justified by: (1) a slight droplet overflow, (2) various dilutions leading to deviations in concentration and (3) the cleavage of sample before the ICP-MS measurements. Moreover, the literature demonstrated that there is no ion leaching during water depollution by photocatalysis with iron oxide/ZnO [17,27]. Iron existence on ZnO NWs was also

proved by EDS analysis on ZnO-Fe0.06% surface after its use for photocatalysis experiments (Figure 2d).

To conclude, the iron drop method seems to lead to the formation of iron oxide fixed on the ZnO NWs without iron diffusion in ZnO lattice and leaching during the photocatalysis process. The formulation of iron oxide synthesized on ZnO nanostructures is not currently known. However, due to parallels made with literature and some characterisation results, we believe FeOOH and Fe_2O_3 are conjointly present on ZnO surface.

3.2 Photocatalytic efficiency

3.2.1 Photocatalysis under natural sunlight

Methyl Orange was chosen as pollutant to study the photocatalytic efficiency under natural sunlight. In fact, MO is photo-resistant, and no photolysis of MO appeared after a long exposition under natural sunlight [7]. Besides, we already demonstrated that MO is not strongly adsorbed by ZnO nanostructures [7].

Photocatalysis was carried out in an open atmosphere between 10 AM to 3 PM from November to December (in Shenzhen, China). It is clearly observed that ZnO daily reference led to stable degradation rate from 37% to 46% after 5h under natural sunlight (Figure 3). Daily weather conditions justify the slight variation on degradation rate per day. Then, by comparing the daily references to degradation rate obtained with ZnO modified samples in order to correct weather conditions, the benefits of iron oxide deposition on ZnO can be studied. Contrary to what gap value suggested, iron content up to 0.48% led to adverse effects on photocatalysis efficiency. Degradation rate after 5h under sunlight in presence of ZnO-Fe2.65%, ZnO-Fe0.95% or ZnO-Fe0.48% decrease by 12%, 4% and 2% compared to their ZnO daily reference. As observed on Figure 2a, at high iron concentration, a non-homogeneous iron oxide layer on ZnO NWs was formed, in particular on the top of ZnO NWs' "tipis" shape, thus preventing light and pollutants access to a part of the ZnO NWs. It could justify the photocatalytic efficiency decreasing due to the loss in available surface.

Moreover, high iron oxide concentration could lead to the formation of recombination centres, which could also reduce photocatalytic activity [14,17,28].

However, at low concentration levels, iron oxide could decrease the recombination rate thanks to charge separation [27,29,30]. For both FeOOH and Fe_2O_3, the delocalisation pathway of electron-hole pairs with zinc oxide is still in debate [14,15, 19, 22, 27-32]. We hypothesize the most favourable pathway is the delocalisation of the electrons from ZnO CB to iron oxide CB, leading to a decrease in the recombination rate and an increase in hydroxyl radical production. It therefore explains the better efficiency obtained for iron content below 0.48%. Furthermore, iron oxide could also participate in photocatalysis and produce hydroxyl radicals [32,33], thus improving the MO degradation. Although, iron oxide could degrade MO by photo-Fenton process thanks to H_2O_2 generated by photocatalysis mechanisms. In fact, Fe_2O_3 efficiency to remove MO by photo-Fenton process under visible light was already proven [34]. Nevertheless, considering the supposed very low production of H_2O_2 by photocatalysis, we can assume that the last point cited will not be the most favourable degradation and improvement pathway, as a matter of fact, the photo-Fenton process needs adding H_2O_2 to enhance depollution rate [35]. Degradation rate after 5h under sunlight in presence of ZnO-Fe0.22%, ZnO-Fe0.06%, ZnO-Fe0.03% increase by 8%, 11% and 6% compared to their ZnO daily reference. Thus, it implies that ZnO-Fe0.06% is the optimal sample for MO degradation under natural sunlight.

Despite the impossibility to make direct comparison with previous results due to the non-identical experimental conditions, it is important to put results into perspective. 200 mL of MO at 10 ppm treated by 50 mg of pure and reduced ZnO powder in suspension under solar light (500 W, Xe lamp) were depolluted at around 35% and 87%, respectively, after 120 min [36]. 50 mL of MO at 200 mg/L were decolorized at 98% after 4 min by photo-Fenton reaction with 1.0 g/L of α-Fe_2O_3 nanoparticles in suspension [34]. 50 mL of MO at 10 mg/L treated by 50 mg of ZnO nanoparticles, TiO_2 NWs, and TiO_2 (B) biphase NWs / ZnO nanoparticle heterojunction (20% weight) under solar

light (300W, Xe lamp) lead to a degradation of 80%, 31% and 100% after 70 min, respectively [37]. Results presented correspond to suspended catalyst, justifying the better degradation efficiency than for the fixed catalyst. Indeed, 200 mL of MO at 10 ppm treated by 0.05 g of ZnO nanoparticles in suspension under natural sunlight (Wuhu, Anhui province, China, July 2010) were totally degraded after 40 min, whereas only 74% of degradation was reached after 6h with ZnO nanoparticles immobilized on a polymeric membrane [38]. Moreover, the weak weight of fixed photocatalyst introduced, less than 1 mg, could also justify the difference between the results issue from different experimental conditions. Taking into account these elements, the recorded results in our work are promising.

3.2.2 Lifetime study

Afterwards, the ZnO-Fe0.06% lifetime was investigated and compared to the ZnO lifetime. To achieve this, 5 cycles of MO degradation were carried out without sample thermal regeneration. Although ZnO-Fe0.06% led to 100% of MO degradation under UV light after 3h as ZnO sample, its kinetic is slower than the ZnO one (Figure 4(a)). This result is coherent with the decrease of UV light absorbed by the samples due to iron oxide layer on the ZnO surface (Figure 2). This finding is also in accordance with literature [15,39].

No losses of kinetic and total degradation rate were recorded for both samples after 5 cycles with a constant degradation rate at 100% after 3h under irradiation (Figure 4(b)).Nevertheless, even if no lack of efficiency was recorded, sample damages appeared on the surface (Figure 4(c)). At first sight, ZnO-Fe0.06% samples seem to be more damaged than reference ZnO. It was clearly confirmed by SEM image. However, on the contrary to what we could expected, ZnO covered by iron oxide seems to be more protected than uncovered ZnO. EDS spectrum (Figure 4c) seems to be consistent with this hypothesis. Iron oxide could act locally as a ZnO photocorrosion protector [20]. By drawing parallels with ZnO/C60 allowing the ZnO photocorrosion reduction, thanks to an

inking of C60 on ZnO vacant sites [40], we can suspect that the iron oxide will also ink on those sites leading to a reduction in oxygen activation and thus photocorrosion (Equations from 2 to 6).

$ZnO + h\nu \rightarrow e^- + h^+$ (2)

$O^{2-}_{surface} + h^+ \rightarrow O^-_{surface}$ (3)

$O^-_{surface} + 3O^{2-} + 3h^+ \rightarrow 2(O - O^{2-})$ (4)

$(O - O^{2-}) + 2h^+ \rightarrow O_2$ (5)

$2Zn^{2+} \rightarrow 2Zn^{2+}_{(aq)}$ (6)

Unfortunately, this punctual presence also seems to be the reported cause of the non-protected ZnO photocorrosion acceleration. A possible explanation to this finding is that iron oxide is supposed to prefer electrons than holes from ZnO. Thus, holes in ZnO will be less recombined and their concentration will increase causing more photocorrosion by the mechanism described by the Equations 7 and 8:

$H_2O + 2h^+ \rightarrow 2H^+ + {}^1/_2\, O_2$ (7)

$ZnO + 2H^+ \rightarrow Zn^{2+} + H_2O$ (8)

We want to emphasize that no strong photocorrosion under natural sunlight, nor under UV light, was observed, even after more than 10h of use for modified ZnO and 25h of using for the ZnO reference (Figure 2a). Therefore, it is possible to assume the photocorrosion observed under UV light is strongly related to the powerful UV light (35 mW/cm² corresponding to 20 suns), which accelerated damage, especially in water. In fact, 18h under UV light exposure in open atmosphere did not lead to any photocorrosion.

Thus, the obtained results are promising for the development of photocatalytic civil engineering materials under natural sunlight, but a small optimisation of the iron homogeneous deposition is needed. Therefore, by a simple improvement of the first deposition process, it will be possible to enhance the photocatalysis under natural sunlight and to protect ZnO against photocorrosion.

4. Conclusion

In this work, a simple "droplet, drying and calcination" method of ferric solution on the surface of ZnO nanostructures was developed as an alternative solution to classical ZnO iron doping for photocatalytic activity improvement. The relevance of this solution was evaluated at the laboratory scale on Si surfaces as substrates. At this small scale on Si surfaces, this process has shown its effectiveness to extend the range of absorbed light thanks to the deposition of iron oxide on ZnO NWs leading to a decrease of the gap value from 3.27 eV to 3.14 eV and higher visible light absorption with iron oxide deposition. Iron oxide phase was not determined, but strong assumptions on the FeOOH and Fe_2O_3 combined presence were made. Modified ZnO with an optimal ratio of 0.06% (Fe *vs* Zn M) improved the photocatalytic efficiency under natural sunlight with an increase of 11% MO degradation, compared to the MO degradation with ZnO reference, after 5h of irradiation with no iron leaching. However, an improvement of the method in order to obtain a homogeneous deposition seems necessary in view of the observed results, especially looking to the photocorrosion where the non-homogeneous covering of iron oxide on ZnO NW surfaces leads a local protection and conversely localized strong photocorrosion of ZnO NWs. Nevertheless, no loss of photocatalytic efficiency were recorded on MO degradation after several cycles of use. Besides, the strong photocorrosion was only recorded under a strong UV light source in water media. These results are promising, but it is necessary to adjust the experimental conditions for a homogeneous functionalization of construction materials such as concrete and tiling substrates, in order to validate this method as an alternative solution to ZnO classical iron doping by insertion of ferric ions in the growth solution.

Acknowledgements

This study was funded by the ‘‘I-Street" project (2017, ADEME via the Programme Investissements d'Avenir, France). Additional support was from the Program No. 2017ZT07Z479,

and from National Natural Science Foundation of China (project No. 42007318). The financial and technical support linked to this project provided are gratefully acknowledged.

Author Contributions

Marie Le Pivert: Synthesis, Realisation of SEM and ICP-MS characterization and photocatalysis experiments, Conceptualization, Writing – original draft and review, Investigation, Formal analysis, Validation, **Hongri Suo:** Conceptualization, Investigation, **Gang Tang:** XRD and ICP-MS sample characterisation, **Han Qiao:** SEM and ICP-MS sample characterisation, **Zhicheng Zhao:** bandgap measurements, **Nathan Martin:** Synthesis, **Chongxuan Liu:** Supervision, Funding acquisition, **Yamin Leprince-Wang:** Conceptualization, Writing – review & editing, Project administration, Funding acquisition.

Competing interests

The authors declare no competing interests.

References

[1] M.Z. Guo, T.C. Ling, C. S. Poon, Photocatalytic NO_X degradation of concrete surface layers intermixed and spray-coated with nano-TiO_2: Influence Of experimental factors, Cem. Concr. Compos. 83 (2017) 279-289. https://dx.doi.org/10.1016/j.cemconcomp.2017.07.022.

[2] L. Senff, D.M. Tobaldi, P. Lemes-Rachadel, J.A. Labrincha, D. Hotza, The influence of TiO_2 and ZnO powder mixtures on photocatalytic activity and rheological behaviour of cement pastes, Constr. Build. Mater. 65 (2014) 191-200. https://doi.org/10.1016/j.conbuildmat.2014.04.121.

[3] V.P. Singh, K. Sandeep, H.S. Kushwaha, S. Powar, R. Vaish, Photocatalytic, hydrophobic and antimicrobial characteristics of ZnO nano needle embedded cement composites, Constr. Build. Mater. 185 (2018) 285-294. https://doi.org/10.1016/j.conbuildmat.2017.10.035.

[4] E. Cerro-Prada, S. Garcia-Salgado, M. A. Quijano, F. Varela, Controlled Synthesis and Microstructural Properties of Sol-Gel TiO_2 Nanoparticles for Photocatalytic Cement Composites, Nanomater. 9 (2018) 1-16. https://doi.org/10.3390/nano9010026.

[5] R.K. Nath, M.F.M Zain, M. Jamil, An environment-friendly solution for indoor air purification by using renewable photocatalyst in concrete: A review, Renew. Sust. Energ. Rev. 62 (2016) 1184-1194. https://doi.org/10.1016/j.rser.2016.05.018.

[6] M. Le Pivert, R. Poupart, M. Capochichi-Gnambodoe, N. Martin, Y. Leprince-Wang, 2019. Direct Growth of ZnO Nanowires on Civil Engineering Materials: Smart Materials for Supported Photodegradation. Microsyst. Nanoeng. 5,57. https://doi.org/10.1038/s41378-019-0102-1.

[7] M. Le Pivert, B. Zerelli, N. Martin, M. Capochichi-Gnambodoe, Y. Leprince-Wang, 2020. Smart ZnO decorated optimized engineering materials for water purification under natural sunlight. Constr. Build. Mater. 257, 119592. https://doi.org/10.1016/j.conbuildmat.2020.119592.

[8] Z. Li, R. Yang, F. Bai, C. Li, Z. L. Wang, Cellular level biocompatibility and biosafety of ZnO nanowires, J. Phys. Chem. C. 112 (2008) 20114-20117. https://doi.org/10.1021/jp808878p.

[9] N. Martin, M. Capochichi-Gnambodoe, M. Le Pivert, Y. Leprince-Wang, A comparative study on the photocatalytic efficiency of ZnO nanowires doped by different transition metals, Acta Phys. Pol. A. 135 (2019) 471-474. https://doi.org/10.12693/AphysPolA.135.471.

[10] Y. Zhang, M. K. Ram, E. K. Stefanakos, D. Y. Goswami, Enhanced photocatalytic activity of iron doped zinc oxide nanowires for water decontamination, Surf. Coat. Tech. 217 (2013) 119-123. https://dx.doi.org/10.1016/j.surfcoat.2012.12.001.

[11] M. Cernea,V. Mihalache, E. C. Secu, R. Trusca, V. Bercu, L. Diamandescu, , Structural, morphological, ferromagnetic and photoluminescence properties of Fe-doped ZnO, prepared by hydrothermal route, Superlattices and Microstruct. 104 (2017) 362-373. https://dx.doi.org/10.1016/j.spmi.2017.02.048.

[12] C. Chevalier-César, M. Capochichi-Gnambodoe, Y. Leprince-Wang, Growth mechanism studies of ZnO nanowires arrays via hydrothermal method, App. Phys. A. 115 (2014) 953-960. https://dx.doi.org/10.1007/s00339-013-7908-8.

[13] M. Erfan, L. Gao, M. Le Pivert, M. Ganmbodoe-Capochichi, Y. M. Sabry, D. Khalil, T. Bourouina, Y. Leprince-Wang, 2020. Real-time optical monitoring of zinc-oxide nanowires in-situ growth within a microfluidic chamber. PROC. SPIE BiOS 2020 11235, 112350W. https://doi.org/10.1117/12.2545131.

[14] R.A. Mirzaie, F. Kamrani, A. A. Firooz, A. A. Khodadadi, Effect of α-Fe_2O_3 addition on the morphological, optical and decolorization properties of ZnO nanostructures, Mater. Chem. Phys. 133 (2012) 311-316. https://doi.org/10.1016/j.matchemphys.2012.01.029.

[15] M.L. Maya-Treviño, J.L. Guzmán-Mar, L. Hinojosa-Reyes, N.A. Ramos-Delgado, M.I. Maldonado, A. Hernández-Ramírez, Activity of the ZnO-Fe_2O_3 catalyst on the degradation of Dicamba and 2,4-D herbicides using simulated solar light, Ceramics Internation. 40 (2014) 8701-8708. https://doi.org/10.1016/j.ceramint.2014.01.088.

[16] Y. Zhou, F. Liu, S. Yu, Preparation and photo-catalytic activities of FeOOH/ZnO/MMT composite, Appl. Surf. Sci. 355 (2015) 861-867. https://doi.org/10.1016/j.apsusc.2015.07.030.

[17] M. Chowdhury, M. Ntiribinyange, K. Nyamayaro, V. Fester, Photocatalytic activities of ultra-small β-FeOOH and TiO_2 heterojunction structure under simulated solar irradiation, Mater. Res. Bull. 68 (2015) 133-141. https://doi.org/10.1016/j.materresbull.2015.03.044.

[18] L. Yin, D. Zhang, J. Wang, J. Huang, X. Kong, J. Fang, F. Zhang, Improving sunlight-driven photocatalytic activity of ZnO nanostructures upon decoration with Fe(III) cocatalyst, Mater. Charact. 127 (2017) 179-184. https://doi.org/10.1016/j.matchar.2017.03.004.

[19] X. Li, B. Jin, J. Huang, Q. Zhang, R. Peng, S. Chu, Fe_2O_3/ZnO/$ZnFe_2O_4$ composites for the efficient photocatalytic degradation of organic dyes under visible light, Solid State Sci. 80 (2018) 6-14. https://doi.org/10.1016/J.solidstatessciences.2018.03.016.

[20] Z. Li , S. Feng, S. Liu, X. Li, L. Wang, W. Lu, A three-dimensional interconnected hierarchical FeOOH/TiO_2/ZnO nanostructural photoanode for enhancing the performance of photoelectrochemical water oxidation, Nanoscale 7 (2015) 19178-19183. https://doi.org/10.1039/C5NR06212H.

[21] W. Shi, T. Gao, L. Zhang, Y. Ma, Z. Liu, B. Zhang, Tailoring the surface structures of iron oxide nanorods to support Au nanoparticles for CO oxidation, Chin. J. Catal. 40 (2020) 1884-1894. https://doi.org/10.1016/S1872-2067(19)63374-7.

[22] F. Achouri, S. Corbel, A. Aboulaich, L. Balan, A. Ghrabi, M. Ben Said, R. Schneider, Aqueous synthesis and enhanced photocatalytic activity of ZnO/Fe_2O_3 heterostructures, J. Phys. Chem. Solids 75 (2014) 1081-1087. https://doi.org/10.1016/j.jpcs.2014.05.013.

[23] Y. Qiu, D. Yang, J. Lei, H. Zhang, I. Ji, B. Yin, J. Bian, Y. Zhao, L. Hu, 2014. Controlled growth of ZnO nanorods on common paper substrate and their application for flexible piezoelectric nanogenerators. J. Mater. Sci.: Mater. Elec. 25, 6. https://doi.org/10.1007/s10854-014-1924-0

[24] P. Wasik, C. Redeker, T. G. Dane, A. M. Seddon, H. Wu, W. H. Briscoe, Hierarchical surface patterns upon evaporation of a ZnO nanofluid droplet: effect of particle morphology, Langmuir 34 (2018) 1645-1654. https://doi.org/10.1021/acs.langmuir.7b03854.

[25] A. Hernández, L. Maya, A. Sánchez-Mora, E. M. Sánchez, Sol-gel synthesis, characterization and photocatalytic activity of mixed oxide ZnO-Fe_2O_3, J. Sol-Gel Sci. Tech. 42 (2007) 71-78. https://doi.org/10.1007/s10971-006-1521-7.

[26] L. Zhang, H. Li, B. Yang, N. Han, Y. Wang, Z. Zhang, Y. Zhou, D. Chen, Y. Gao, Promote the electrocatalysis activity of amorphous FeOOH to oxygen evolution reaction by coupling with ZnO nanorod array, J. Solid State Electrochem. 24 (2020) 905-914. https://doi.org/10.1007/s10008-020-04540-2.

[27] G.K. Pradhan, S. Martha, M. Parida, Synthesis Of Multifunctional Nanostructured Zinc−Iron Mixed Oxide Photocatalyst by a Simple Solution-Combustion Technique, Appl. Mater. Interface 4 (2011) 707-713. https://doi.org/10.1021/am201326b.

[28] J. Xie, L. Zhang, M. Li, Y. Hao, Y. Lian, Z. Li, Y. Wei, α-Fe_2O_3 modified ZnO flower-like microstructures with enhanced photocatalytic performance for pentachlorophenil degradation, Ceramics Internation. 41 (2015) 9420-9425. https://doi.org/10.1016/j.ceramint.2015.03.320.

[29] Q. Yin, R. Qia, L. Zhu, Z. Li, M. Li, W. Wu, α-Fe_2O_3 decorated ZnO nanorod-assembled hollow microspheres: Synthesis and enhanced visible-light photocatalysis, Mater. Lett. 135 (2014) 135-138. https://doi.org/10.1016/j.matlet.2014.07.149.

[30] Y. Liu, L. Sun, J. Wu, T. Fang, R. Cai, A. Wei, Preparation and photocatalytic activity of ZnO/Fe_2O_3 nanotube composites, Mater. Sci. and Eng. B 194 (2015) 9-13. https://doi.org/10.1016/j.mseb.2014.12.021.

[31] W. Yan, H. Fan, C. Yang, Ultra-fast synthesis and enhanced photocatalytic properties of alpha-Fe_2O_3/ZnO core-shell structure, Mater. Lett. 65 (2011) 1595-1597. https://doi.org/10.1016/j.matlet.2011.03.026.

[32] Y. Liu, L. Yu, Y. Hu, C. Guo, F. Zhang, X. W. Lou, A magnetically separable photocatalyst based on nest-like γ-Fe_2O_3/ZnO double-shelled hollow structures with enhanced photocatalytic activity, Nanoscale 4 (2012) 183-187. https://doi.org/10.1039/C1NR11114K.

[33] A. Benaboud, M. Zaabat, M.S. Aida, B. Boudine, S. Benzitouni, T. Saidani, Fe_2O_4/ZnO-nanowires synthesis by dip-coating for orange II-dye photodegradation, Optik 144 (2017) 397-405. https://doi.org/10.1016/J.IJLEO.2017.06.108.

[34] H. Xiang, G. Ren, X. Yang, D. Xu, Z. Zhang, X. Wang, 2020. A low-cost solvent-free method to synthesize α- Fe_2O_3 nanoparticules with applications to degrade methyl orange in photo-fenton system. Ecotox. Environ. Safe. 200,110744. https://doi.org/10.1016/j.ecoenv.2020.110744.

[35] V.V. Pham., V. C. Duong, Q. H. Nguyen, N. D. Nguyen, M. T. Cao, Visible-light-induced photo-Fenton degradation of rhodamine B over Fe_2O_3-diatomite materials, J. Sci.: Adv. Mater. Devices 5 (2020) 308-315. https://doi.org/10.1016/j.jsamd.2020.07.007.

[36] M.H. Farooq, I. Aslam, H.S. Anam, M. Tanveer, Z. Ali, U. Ghani, R. Boddula, Improved photocatalytic performance of reduced zinc oxide (ZnO) novel morphology of astray like microstructure under solar light irradiation, Mater. Sci. Energy Technol. 2 (2019) 181–186. https://doi.org/10.1016/j. mset.2019.01.005.

[37] C. Sun, Q. Xu, Y. Xie, Y. Ling, Y. Hou, Designed synthesis of anatase–TiO_2 (B) biphase nanowire/ZnO nanoparticle heterojunction for enhanced photocatalysis, J. Mater. Chem. A 6 (2018) 8289-8298. https://doi.org/10.1039/C7TA10274G.

[38] B. Hu, J. Zhou, X.M. Wu, 2013. Decoloring methyl orange under sunlight by a photocatalytic membrane reactor based on ZnO nanoparticles and polypropylene microporous membrane, Int. J. Polym. Sci. 2013, 451398. https://doi.org/10.1155/2013/451398.

[39] S. Yang, Q. Xie, X. Li, Y. Liu, S. Chen, G. Chen, Preparation, characterization and photoelectrocatalytic properties of nanocrystalline Fe_2O_3/TiO_2, ZnO/TiO_2, and $Fe_2O_3/ZnO/TiO_2$ composite film electrodes towards pentachlorophenol degradation, Phys. Chem. Chem. Phys. 6 (2004) 659-664. https://doi.org/10.1039/B308336E.

[40] H. Fu, T. Xu, S. Zhu, Y. Zhu, Photocorrosion Inhibition and Enhancement of Photocatalytic Activity for ZnO via Hybridization with C60, Environ. Sci. Tech. 42 (2008) 8064-8069. https://doi.org/10.1021/es801484x.

Table

Table. 1. Resume of gap values, iron theoretical and measured concentrations and molar ratios of ZnO modified sample with iron.

Sample name	Gap (eV)	$[Fe]_{theoretical}$ (mol)	$[Fe]_{estimated\ by\ ICP\text{-}MS}$ (mol)
ZnO-Fe2.65%	3.14	4.46×10^{-7}	3.80×10^{-7}
ZnO-Fe0.95%	3.16	1.79×10^{-7}	1.40×10^{-7}
ZnO-Fe0.48%	3.21	8.93×10^{-8}	6.58×10^{-8}
ZnO-Fe0.22%	3.24	4.46×10^{-8}	1.42×10^{-8}
ZnO-Fe0.06%	3.25	1.79×10^{-8}	5.42×10^{-9}
ZnO-Fe0.03%	3.27	8.93×10^{-9}	3.05×10^{-9}

List of figure captions

Figure 1. Pictures of iron / substrate interaction **(a),** Photocatalysis degradation rate as function of time for Acid Red 14 under natural sunlight in presence of ZnO and Fe doped ZnO on tiling substrate (10 µM, V = 30 mL) **(b)**.

Figure 2. SEM top-view pictures **(a)**, UV-visible spectral plot with Tauc-Lorentz model **(b)**, and XRD pattern **(c)** of unmodified and modified ZnO; EDS spectrum on ZnO-Fe0.06% after several degradation cycles under sunlight **(d)**.

Figure 3. Photocatalysis degradation rate as function of time for MO under natural sunlight in presence of unmodified and modified ZnO.

Figure 4. Photocatalytic degradation rate of MO under UV light in presence of ZnO and ZnO-Fe0.06% for the cycle 1 **(a)** and for subsequent experiment cycles **(b)**; SEM top-view pictures of ZnO and ZnO-Fe0.06% after five experiment cycles (> 18h) **(c)**.

Figures

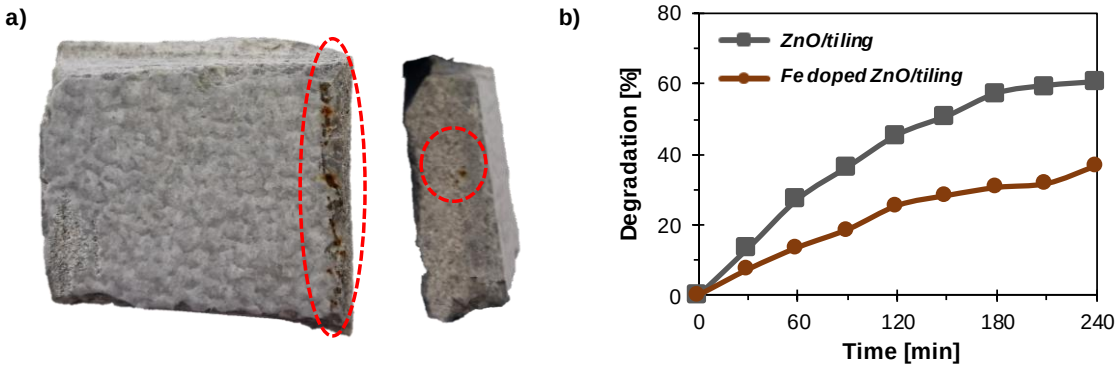

Figure 1

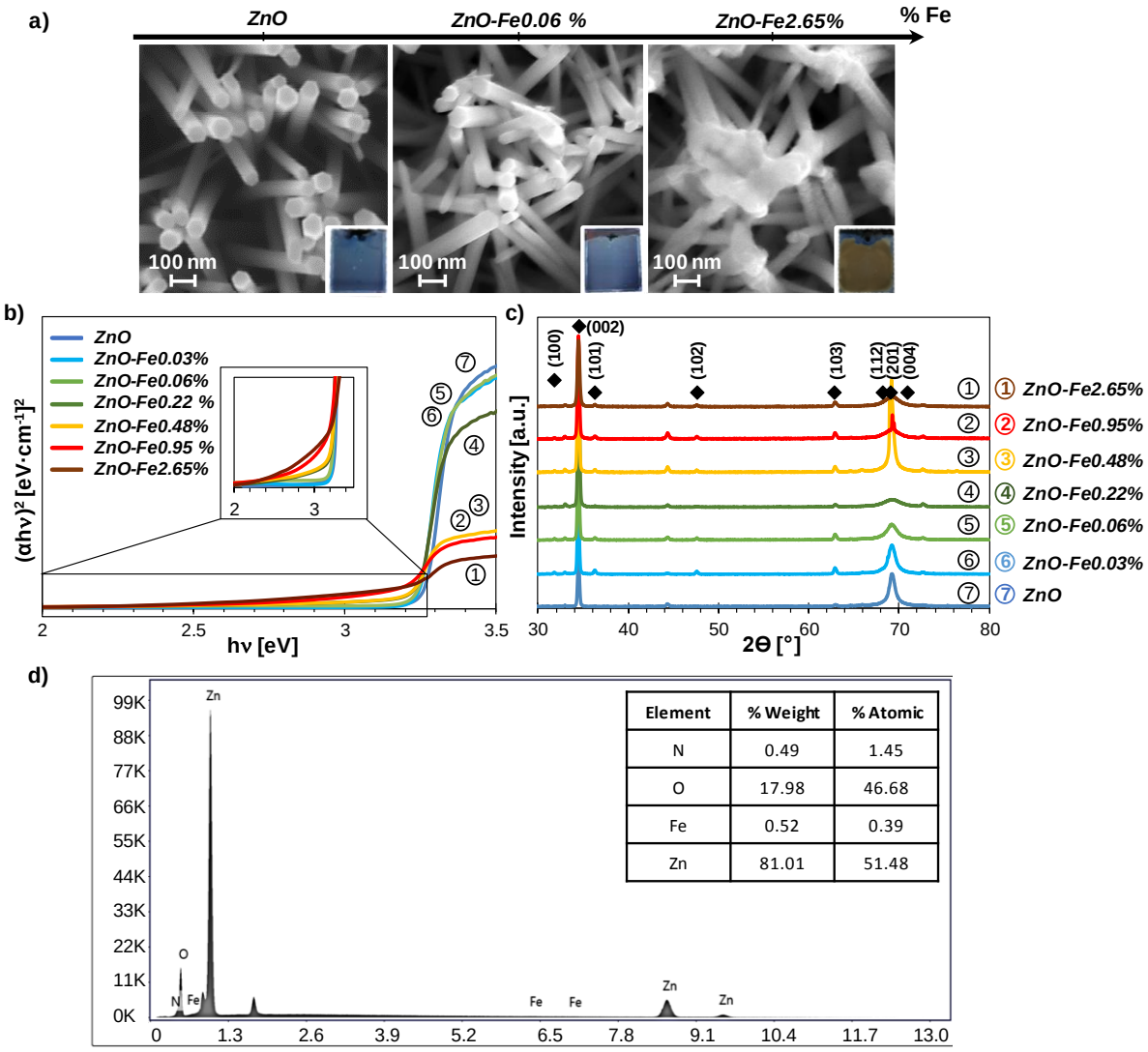

Element	% Weight	% Atomic
N	0.49	1.45
O	17.98	46.68
Fe	0.52	0.39
Zn	81.01	51.48

Figure 2

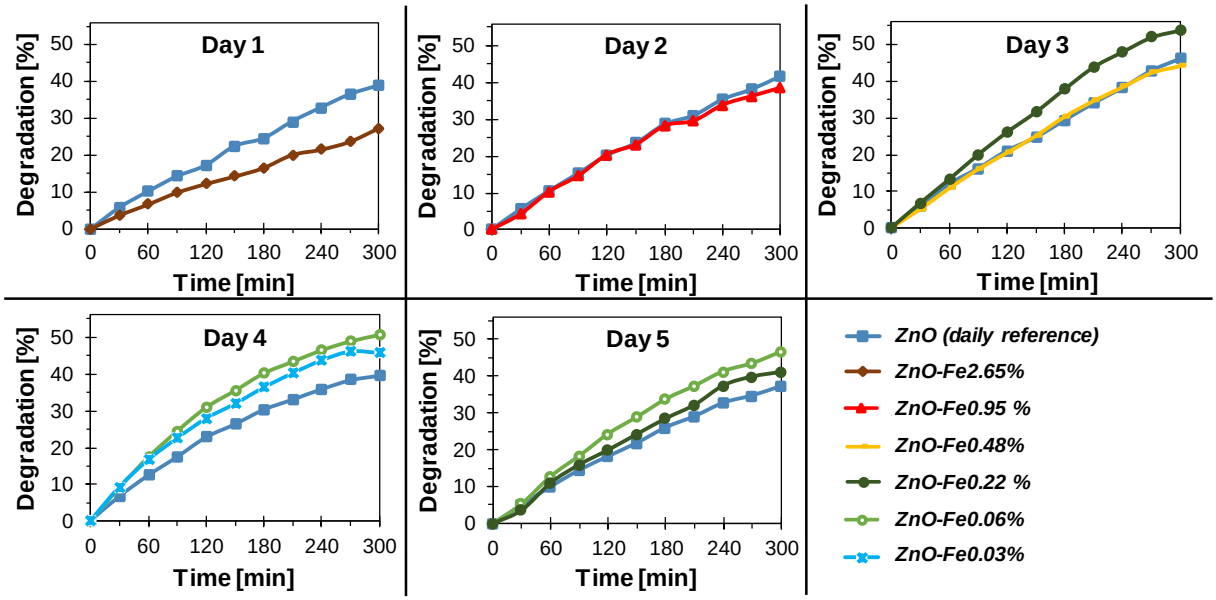
Day 1
Day 2
Day 3
Day 4
Day 5
Degradation [%]
Time [min]
0
10
20
30
40
50
0
60
120
180
240
300
ZnO (daily reference)
ZnO-Fe2.65%
ZnO-Fe0.95 %
ZnO-Fe0.48%
ZnO-Fe0.22 %
ZnO-Fe0.06%
ZnO-Fe0.03%

Figure 3

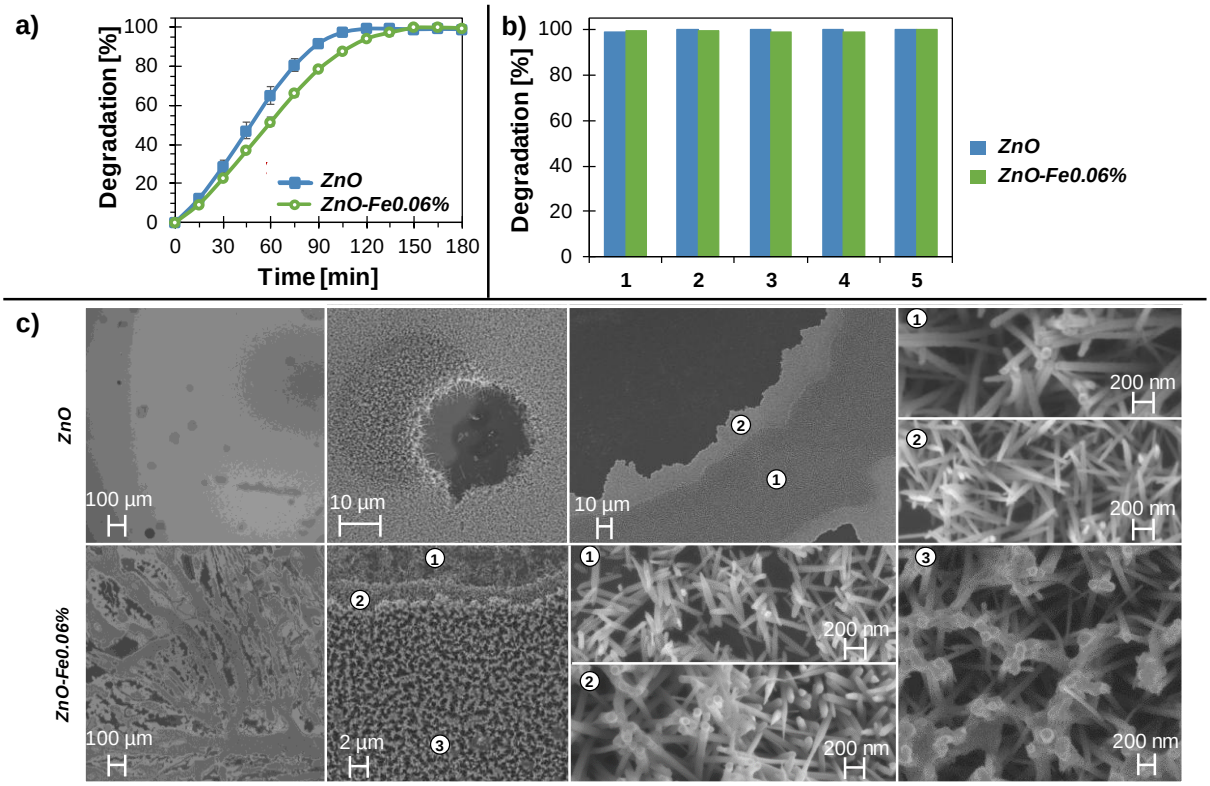
a)
Degradation [%]
100
80
60
40
20
0
0 30 60 90 120 150 180
Time [min]
ZnO
ZnO-Fe0.06%
b)
Degradation [%]
100
80
60
40
20
0
1 2 3 4 5
ZnO
ZnO-Fe0.06%
c)
ZnO
ZnO-Fe0.06%
100 µm
10 µm
10 µm
200 nm
200 nm
100 µm
2 µm
200 nm
200 nm
200 nm

Figure 4